RSC Applied Interfaces

ROYAL SOCIETY OF CHEMISTRY

PAPER

View Article Online
View Journal | View Issue

Cite this: *RSC Appl. Interfaces*, 2026, 3, 837

Effect of temperature dependence of deformation polarizability and ionization energy of solvents on surface properties of solid materials

Tayssir Hamieh [abc]

In recent studies, an original approach based on the London interaction equation has been proposed for the determination of the dispersive and polar surface properties of solid materials. The reported results revealed significant deviations in surface parameters compared with those obtained using classical methods. However, in these earlier works, the ionization energy and the deformation polarizability of solids and probe molecules were assumed to be temperature-independent. In the present work, the effect of temperature on these two fundamental molecular parameters is investigated, and the influence of their temperature dependence on the surface properties associated with the adsorption of organic solvents on oxide materials such as alumina, titania, and magnesium oxide is examined. Inverse gas chromatography (IGC) at infinite dilution is employed to determine the net retention volumes of probe molecules, enabling the calculation of the free energy of adsorption, as well as its dispersive and polar components, the Lewis acid–base parameters, and the corresponding surface energies. The results demonstrate that thermal variations in ionization energy and deformation polarizability—although relatively small—have a pronounced impact on surface thermodynamic parameters. In particular, changes of up to 100% are observed in the dispersive and polar components of the adsorption free energy for several probe molecules, while variations in the Lewis acid–base constants of solid surfaces reach up to 200% in the case of magnesium oxide. These findings clearly highlight the high sensitivity of surface properties to temperature-dependent molecular parameters and emphasize the necessity of explicitly accounting for thermal effects in the analysis of surface–molecule interactions.

Received 9th January 2026,
Accepted 12th April 2026

DOI: 10.1039/d6lf00006a

rsc.li/RSCApplInter

1. Introduction

In a previous study,[1] an original method was introduced to determine the surface properties of solid materials by exploiting the London dispersion interaction energy between model organic probe molecules and solid surfaces. This approach enabled a more accurate separation of dispersive and polar contributions to the adsorption free energy, leading to a significant correction of the Lewis acid–base parameters of solid surfaces compared with classical chromatographic models. Such an improved separation is of considerable importance for the reliable prediction of physicochemical surface properties of materials and nanomaterials.[1]

Inverse gas chromatography (IGC) at infinite dilution has been widely employed to quantify dispersive and polar free energies of adsorption through the measurement of retention volumes of probe molecules on solid materials.[2–46] In this framework, the standard free energy of adsorption, $\Delta G_a^0(T)$, is determined as a function of temperature. The London-equation-based approach has demonstrated clear superiority over traditional methods relying on empirical or semi-empirical solvent parameters, such as the boiling point T_{BP},[2] vapor pressure P_0,[3,4] dispersive surface tension γ_l^d,[8] topological indices,[6,7] standard enthalpy of vaporization ΔH_{vap}^0, or deformation polarizability $\alpha_{0,L}$.[5]

Several subsequent studies[1,8,13–17,26,27,34] have further refined the determination of surface properties—including dispersive surface energy, polar free energy, and Lewis acid–base constants—by incorporating thermal models that account for the temperature dependence of the surface area of organic probe molecules. These developments have confirmed the essential role of temperature in surface thermodynamics.

More recently, the London-equation-based formalism introduced a new thermodynamic parameter, $\mathcal{P}_{SX}$, to describe solid–molecule interactions, defined as:

[a] *Faculty of Science and Engineering, Maastricht University, 6200 MD Maastricht, The Netherlands. E-mail: t.hamieh@maastrichtuniversity.nl*
[b] *Institut de Science des Matériaux de Mulhouse, Université de Haute-Alsace, CNRS, IS2M UMR 7361, F-68100 Mulhouse, France*
[c] *Laboratory of Materials, Catalysis, Environment and Analytical Methods (MCEMA), Faculty of Sciences, Lebanese University, P.O. Box 6573/14, Beirut, Lebanon*

$$\mathcal{P}_{SX} = \frac{3}{2}\frac{\mathcal{N}\alpha_{0S}\alpha_{0X}}{(4\pi\varepsilon_0)^2}\frac{\varepsilon_S\varepsilon_X}{(\varepsilon_S+\varepsilon_X)} \quad (1)$$

where α_{0S} and α_{0X} are the deformation polarizabilities of the solid surface and the adsorbed molecule, respectively, $\mathcal{N}$ is Avogadro's number, ε_0 is the vacuum permittivity, and ε_S and ε_X are their corresponding ionization energies. In previous applications of this model, both deformation polarizability and ionization energy were assumed to be independent of temperature.

In the present work, this framework is extended by explicitly considering the temperature dependence of deformation polarizability and ionization energy for both solids and probe molecules. This refined approach is applied to the determination of surface properties of alumina, titania, and magnesium oxide, examining its impact on the dispersive and polar components of the adsorption free energy, the Lewis acid–base parameters, and the corresponding acid and base surface energies. This study provides a more physically consistent description of surface–molecule interactions and highlights the critical role of thermal effects in surface thermodynamic analyses.

2. Materials and methods

The solid materials and organic solvents were used in previous studies[1,16,17] using chromatographic methods and models. The non-polar organic solvents were *n*-hexane, *n*-heptane, *n*-octane, and n-nonane, whereas the polar molecules were dichloromethane, chloroform, carbon tetrachloride, benzene, ethyl acetate, diethyl ether, acetone, tetrahydrofuran (THF), acetone, toluene, and acetonitrile.

In the context of inverse gas chromatography, molecular polarity is not solely defined by the presence of a permanent dipole moment. According to the Gutmann donor–acceptor concept, molecules such as benzene, toluene, and carbon tetrachloride—although nonpolar in the classical electrostatic sense—exhibit weak but measurable electron-donor or electron-acceptor character arising from π-electron delocalization or highly polarizable bonds. These molecules are therefore treated as weakly polar probes in IGC analyses, as they are capable of engaging in specific Lewis acid–base interactions with solid surfaces. Table S1 summarizes the corrected Gutmann donor (DN) and acceptor (AN) electron numbers together with the permanent dipole moments of the probe molecules, highlighting that several solvents classified as weakly polar or amphoteric in inverse gas chromatography exhibit specific Lewis acid–base character despite possessing negligible or very small permanent dipole moments.

The solid materials were alumina (Al_2O_3), magnesium oxide (MgO), and titania (TiO_2) and previously characterized.[1] Table 1 lists for all chemicals the CAS registry number, source of chemicals, and reported purity. The net retention time of organic solvents adsorbed on the different solid surfaces was determined at different temperatures using inverse gas chromatography (IGC) at infinite dilution with the help of a Focus GC gas chromatograph equipped with a flame ionization detector of high sensitivity (Sigma-Aldrich, Paris, France). A mass of 1 g of solid particles was packed into a stainless-steel column of a length of 30 cm and 2 mm internal diameter. Helium was used as carrier gas with a flow rate equal to 25 mL min^{-1}. The retention times of the different injected organic solvents were measured at infinite dilution, supposing that there is no interaction between the probe molecules themselves. The column temperatures varied from 30 to 200 °C. Average retention times and volumes were determined by repeating each solvent injection three times with a standard deviation less than 1% in all chromatographic measurements. Uncertainty propagation was evaluated by considering experimental uncertainties in retention times (1%), temperature control (±0.1 K), and molecular parameters such as deformation polarizability and ionization energy. The resulting uncertainties in derived adsorption energies and acid–base parameters remain within ±5%, indicating that the observed temperature trends are

Table 1 List of probe molecules used in this study with CAS registry number, source of chemicals, and reported purity. All chemicals were used as received without further purification

Chemical	CAS no.	Supplier and location	Reported purity
n-Hexane	110-54-3	Aldrich, Paris, France	≥99%
n-Heptane	142-82-5	Aldrich, Paris, France	≥99%
n-Octane	111-65-9	Aldrich, Paris, France	≥99%
n-Nonane	111-84-2	Aldrich, Paris, France	≥99%
Dichloromethane	75-09-2	Aldrich, Paris, France	≥99%
Chloroform	67-66-3	Aldrich, Paris, France	≥99%
Carbon tetrachloride	56-23-5	Aldrich, Paris, France	≥99%
Benzene	71-43-2	Aldrich, Paris, France	≥99%
Ethyl acetate	141-78-6	Aldrich, Paris, France	≥99%
Diethyl ether	60-29-7	Aldrich, Paris, France	≥99%
Acetone	67-64-1	Aldrich, Paris, France	≥99%
Tetrahydrofuran (THF)	109-99-9	Aldrich, Paris, France	≥99%
Toluene	108-88-3	Aldrich, Paris, France	≥99%
Acetonitrile	75-05-8	Aldrich, Paris, France	≥99%
α-Alumina (Al_2O_3)	1344-28-1	Aldrich, Paris, France	≥99%
Magnesium oxide (MgO)	1309-48-4	Aldrich, Paris, France	≥99%
Titanium dioxide (TiO_2)	13463-67-7	Aldrich, Paris, France	≥99%

robust and not dominated by experimental error. All reported values represent the mean of repeated measurements, and the associated uncertainties are expressed as standard deviations. The number of significant figures has been adjusted to reflect the experimental precision.

The IGC technique[2–46] allows the characterization of the surface properties of solid materials through the determination of the net retention volumes of probe molecules adsorbed on the solid surfaces. This approach enables the determination of the free energy of adsorption ΔG_a^0 of the adsorbed molecules by using the following fundamental equation of IGC:

$$\Delta G_a^0(T) = -RT \ln V_n + C(T) \quad (2)$$

where V_n is the net retention volume of a probe, T the absolute temperature, R the universal gas constant, and $C(T)$ a constant depending on the temperature and the parameters of interaction between the solid and the solvent given by:

$$\left(-\frac{\Delta H^p}{AN}\right) = K_A\left(\frac{DN}{AN}\right) + K_D \quad (3)$$

where m is the mass of the solid particles, s is the specific surface area of the solid material, and P_0 is the reference pressure, while π_0 is the two-dimensional pressure defined in the literature according to one of the following reference states:

- Kemball and Rideal reference state[47] given for T_0 = 0 °C by $P_0 = 1.013 \times 10^5$ Pa and $\pi_0 = 6.08 \times 10^{-5}$ N m^{-1}.

- De Boer and Kruyer reference state[48] given for T_0 = 0 °C by $P_0 = 1.013 \times 10^5$ Pa and $\pi_0 = 3.38 \times 10^{-5}$ N m^{-1}.

The total free energy of adsorption $\Delta G_a^0(T)$ is composed of the respective London dispersive energy $\Delta G_a^d(T)$ and polar energy $\Delta G_a^p(T)$:

$$\Delta G_a^0(T) = \Delta G_a^d(T) + \Delta G_a^p(T) \quad (4)$$

In a recent study, an original method based on the London dispersion interaction expression was proposed.[34] The London dispersion eqn (1) was used for the determination of the free dispersive energy $-\Delta G_a^d(T)$ and the fundamental equation is written as:

$$\Delta G_a^d(T) = -\frac{3}{2}\frac{\alpha_{01}\alpha_{02}}{(4\pi\varepsilon_0)^2 H^6}\frac{\mathcal{N}\varepsilon_1\varepsilon_2}{(\varepsilon_1+\varepsilon_2)} \quad (5)$$

where α_{01} and α_{02} are the respective deformation polarizabilities of molecules 1 and 2 separated by a distance H, and ε_1 and ε_2 are the ionization energies of molecules 1 and 2.

In the case of adsorption of organic solvents on solid materials, the solid molecule (molecule 1) was denoted S and the probe molecule (molecule 2) denoted by X and combining the previous equations. The free energy of adsorption $\Delta G_a^0(T)$ can be written as:

A new thermodynamic parameter $\mathcal{P}_{SX}$ was proposed as new chromatographic indicator variable given by:

$$\mathcal{P}_{SX} = \frac{3}{2}\frac{\mathcal{N}\alpha_{0S}\alpha_{0X}}{(4\pi\varepsilon_0)^2}\frac{\varepsilon_S\varepsilon_X}{(\varepsilon_S+\varepsilon_X)}$$

eqn (6) becomes as follows:

$$\Delta G_a^0(T) = -RT \ln V_n + C(T) = -\frac{\mathcal{P}_{SX}}{H^6} + \Delta G_a^p(T) \quad (7)$$

The representation of $\Delta G_a^0(T)$ as a function of $\mathcal{P}_{SX}$ led to quantify both the dispersive and polar contributions of the total free energy of adsorption using *n*-alkanes and polar solvents. The free energy of *n*-alkanes gave the dispersive component $\Delta G_a^d(T)$ because they only exhibit dispersive interactions, while the distance between the representative point of the polar solvent and the *n*-alkanes straight-line led to ΔG_a^p as it was shown in Fig. 1.

Knowing the polar free energy of polar solvents and their total free energy, it was possible to obtain the dispersive free energy of these solvents using eqn (4). On the other hand, the application of eqn (5) to n-alkanes and polar organic molecules allowed to determine the separation distance H between the solvents and solid material.

In previous studies,[1,26,27] the ionization energy and deformation polarizability of solid and solvents were supposed constants independent from the temperature. Even if the variations of these variables slightly vary *versus* the temperature, the temperature effect of these parameters on the surface properties of solid materials was highlighted in this paper.

For clarity and consistency, a list of abbreviations, definitions, and units used in the theoretical and thermodynamic analysis is provided in the SI.

3. Results

The variations of the ionization energy and deformation polarizability of the different compounds used in this work were determined as a function of temperature using several references from the literature.[49–64] Recent studies[65–70] further illustrate the growing use of electronic-structure descriptors (*e.g.*, adsorption energies, reaction barriers, charge redistribution, and free-energy relationships) to rationalize chemical reactivity and interfacial phenomena. For example, kinetic and mechanistic analyses of gas-phase radical reactions highlight how electronic features and the underlying potential-energy surface govern reaction pathways and reactivity trends.[65,66] In parallel, density functional theory (DFT) investigations have been widely employed to resolve mechanistic questions by locating transition states and quantifying activation energies, thereby linking molecular electronic structure to measurable thermodynamic

$$\Delta G_a^0(T) = -RT \ln V_n + C(T) = -\frac{\alpha_{0S}}{H^6}\left[\frac{3\mathcal{N}}{2(4\pi\varepsilon_0)^2}\left(\frac{\varepsilon_S\varepsilon_X}{(\varepsilon_S+\varepsilon_X)}\alpha_{0X}\right)\right] + \Delta G_a^p(T) \quad (6)$$

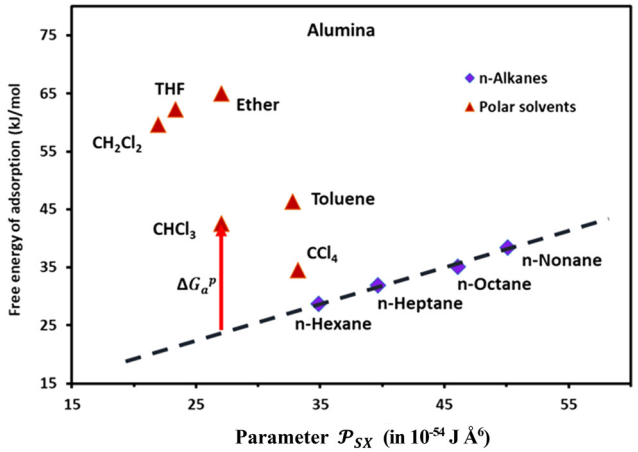

Fig. 1 Variations of the free energy ΔG_a^0 (in kJ mol^{-1}) of adsorption of organic solvents on alumina surfaces as a function of the parameter $\mathcal{P}_{SX}$ (in 10^{-54} J Å^6) at 323.15 K.

and kinetic observables.[65] DFT has also been used to analyze adsorption on carbon-based substrates (*e.g.*, defective graphene), where adsorption-induced changes in electronic properties are central to sensing and interfacial response. Likewise, recent computational studies correlate molecular electronic properties with functional performance, including organic redox/electrode behavior and acid–base descriptors derived from energetic and vibrational signatures.[70] Collectively, these contributions emphasize that surface/interfacial properties are governed by electronic quantities and their coupling to thermodynamic functions. In this context, explicitly incorporating the temperature dependence of ionization energy and deformation polarizability provides a physically consistent route to improve adsorption-energy partitioning and Lewis acid–base surface parameters obtained from inverse gas chromatography.

The values of the deformation polarizability α_0 of solvents and solid materials as a function of temperature were given in Table S2 showing a slight linear increase and satisfying the following equation:

$$\alpha_0(T) = (\mathrm{d}\alpha_0/\mathrm{d}T)T + \alpha_0(0\ \mathrm{K}) \quad (8)$$

where $\mathrm{d}\alpha_0/\mathrm{d}T$ is the temperature coefficient of polarizability and α_0 (0 K) is the deformation polarizability extrapolated at 0 K. The linear equations relative to the solvents and solid surfaces were given in Table 2. It was observed that the polarizability coefficient is the highest for n-alkanes reaching 4.8×10^{-43} C m^2 V^{-1} K^{-1} for n-nonane proving the highest polarizability change with temperature.

The uncertainties associated with the thermal coefficients $\mathrm{d}\alpha_0/\mathrm{d}T$ and deformation polarizability $\alpha_0(T)$ were determined by propagation of the standard deviations obtained from inverse gas chromatography (IGC) measurements. Each probe injection was repeated three times, resulting in an overall relative error of less than 1%.

The variations of the ionization energy $\varepsilon(T)$ of solvents and solid materials were given in Table S3 as a function of temperature. The obtained results showed very slight variations of $\varepsilon(T)$ against the temperature. However, the variations of both $\alpha_0(T)$ and $\varepsilon(T)$ affect the values of the interaction parameter $\mathcal{P}_{SX}$ *versus* the temperature.

The new method was based on the temperature effect on the chromatographic parameter $\mathcal{P}_{SX}$ of different solvents respectively adsorbed on alumina, titania, and magnesium oxide.

Although the International System of Units is used as the reference framework, intermolecular distances are expressed in angstroms for convenience. Accordingly, the parameter $\mathcal{P}_{SX}$ is reported in J Å^6 mol^{-1}, ensuring that the ratio $\mathcal{P}_{SX}/H^6$ retains the correct unit of adsorption free energy (J mol^{-1}).

Table 2 Equations of the deformation polarizability $\alpha_0(T)$ ($\times 10^{-40}$ C m^2 V^{-1}) of solvents and solid materials as a function of temperature with the values of the temperature coefficient of polarizability $\mathrm{d}\alpha_0/\mathrm{d}T$ and those of deformation polarizability α_0 (0 K) ($\times 10^{-40}$ C m^2 V^{-1}) extrapolated at 0 K. Reported uncertainties (±) correspond to standard deviations obtained from the fitting procedure

Compounds	Equation of $\alpha_0(T)$	$\mathrm{d}\alpha_0/\mathrm{d}T$ ($\times 10^{-3}$)	α_0 (0 K)
n-Hexane	$\alpha_0(T) = 2.9 \times 10^{-3}T + 12.378$	2.9 ± 0.03	12.378 ± 0.124
n-Heptane	$\alpha_0(T) = 3.5 \times 10^{-3}T + 14.112$	3.5 ± 0.04	14.112 ± 0.141
n-Octane	$\alpha_0(T) = 4.3 \times 10^{-3}T + 16.420$	4.3 ± 0.04	16.420 ± 0.164
n-Nonane	$\alpha_0(T) = 4.8 \times 10^{-3}T + 17.876$	4.8 ± 0.05	17.876 ± 0.179
CCl_4	$\alpha_0(T) = 2.2 \times 10^{-3}T + 11.410$	2.2 ± 0.02	11.410 ± 0.114
Nitromethane	$\alpha_0(T) = 1.3 \times 10^{-3}T + 7.822$	1.3 ± 0.01	7.822 ± 0.078
CH_2Cl_2	$\alpha_0(T) = 1.2 \times 10^{-3}T + 7.660$	1.2 ± 0.01	7.660 ± 0.077
Chloroform	$\alpha_0(T) = 1.7 \times 10^{-3}T + 9.352$	1.7 ± 0.02	9.352 ± 0.094
Diethyl ether	$\alpha_0(T) = 2.1 \times 10^{-3}T + 9.900$	2.1 ± 0.02	9.900 ± 0.099
THF	$\alpha_0(T) = 1.8 \times 10^{-3}T + 8.602$	1.8 ± 0.02	8.602 ± 0.086
Ethyl acetate	$\alpha_0(T) = 2.5 \times 10^{-3}T + 9.45$	2.5 ± 0.03	9.450 ± 0.095
Acetone	$\alpha_0(T) = 1.1 \times 10^{-3}T + 6.762$	1.1 ± 0.01	6.762 ± 0.068
Acetonitrile	$\alpha_0(T) = 0.7 \times 10^{-3}T + 4.72$	0.7 ± 0.01	4.720 ± 0.047
Toluene	$\alpha_0(T) = 2.4 \times 10^{-3}T + 12.410$	2.4 ± 0.02	12.410 ± 0.124
Benzene	$\alpha_0(T) = 2.1 \times 10^{-3}T + 10.898$	2.1 ± 0.02	10.898 ± 0.109
Alumina	$\alpha_0(T) = 0.3 \times 10^{-3}T + 5.86$	0.3 ± 0.00	5.860 ± 0.059
Titania	$\alpha_0(T) = 0.7 \times 10^{-3}T + 7.71$	0.7 ± 0.01	7.710 ± 0.077
MgO	$\alpha_0(T) = 0.3 \times 10^{-3}T + 6.23$	0.3 ± 0.00	6.230 ± 0.062

Table 3 Values of parameter $\mathcal{P}_{SX}(T)$ of solvents adsorbed on of the solid materials as a function of temperature. The uncertainty associated with $\mathcal{P}_{SX}(T)$ is in the range 0.001–0.012 ($\times 10^{-54}$ J Å^6 mol^{-1})

Parameter $\mathcal{P}_{SX}(T)$ ($\times 10^{-54}$ J Å^6 mol^{-1}) of alumina				
Temperature (K)	323.15	343.15	363.15	383.15
n-Hexane	34.885	35.073	35.261	35.450
n-Heptane	39.639	39.862	40.086	40.309
n-Octane	46.084	46.354	46.624	46.896
n-Nonane	50.093	50.393	50.693	50.993
CCl_4	33.196	33.351	33.505	33.660
CH_2Cl_2	21.941	22.029	22.118	22.206
Chloroform	27.036	27.157	27.278	27.399
Ether	27.060	27.196	27.332	27.468
THF	23.367	23.483	23.599	23.715
Ethyl acetate	26.756	26.914	27.073	27.231
Toluene	32.751	32.904	33.058	33.212
Parameter $\mathcal{P}_{SX}(T)$ ($\times 10^{-54}$ J Å^6 mol^{-1}) of titania				
Temperature (K)	323.15	343.15	363.15	383.15
n-Hexane	60.648	61.029	61.411	61.793
n-Heptane	68.759	69.207	69.656	70.107
n-Octane	79.819	80.358	80.899	81.441
n-Nonane	86.674	87.269	87.866	88.464
CH_2Cl_2	38.621	38.810	39.000	39.190
Chloroform	47.612	47.867	48.122	48.379
THF	40.272	40.508	40.744	40.981
Ethyl acetate	46.454	46.770	47.087	47.405
Acetone	31.743	31.902	32.062	32.222
Benzene	50.392	50.672	50.953	51.234
Nitromethane	39.167	39.365	39.565	39.765
Acetonitrile	24.545	24.661	24.778	24.895
Parameter $\mathcal{P}_{SX}(T)$ ($\times 10^{-54}$ J Å^6 mol^{-1}) of MgO				
Temperature (K)	323.15	343.15	363.15	383.15
n-Hexane	41.560	41.701	41.842	41.982
n-Heptane	47.169	47.340	47.511	47.681
n-Octane	54.795	55.007	55.219	55.429
n-Nonane	59.530	59.767	60.004	60.240
CH_2Cl_2	26.309	26.362	26.415	26.468
Chloroform	32.426	32.506	32.586	32.666
Diethyl ether	32.118	32.215	32.312	32.408
THF	27.712	27.794	27.877	27.958
Ethyl acetate	31.854	31.979	32.103	32.227
Acetone	21.803	21.850	21.896	21.942
Acetonitrile	16.654	16.685	16.716	16.747
Toluene	38.700	38.804	38.908	39.012

Table 3 gave the variations of $\mathcal{P}_{SX}(T)$ as a function of temperature of the adsorbed organic molecules on solid materials using the values given in previous paper.[34] It was observed a slight variation of $\mathcal{P}_{SX}(T)$ *versus* the temperature. However, there is an important variation of $\mathcal{P}_{SX}(T)$ depending on both solvents and solid surfaces. This was more elucidated in Table 4 giving the equations $\mathcal{P}_{SX}(T)$ of the different solvents with the extrapolated values of $\mathcal{P}_{SX}(0\,K)$ at 0 K. $\mathcal{P}_{SX}(0\,K)$ largely varied from solvent to another and from solid to solid. The slope $d\mathcal{P}_{SX}(T)/dT$ which is equal to the derivative of $\mathcal{P}_{SX}$ with respect of temperature represents a thermal expansion coefficient. The general equation was given as follows:

$$\mathcal{P}_{SX}(T) = A + BT \quad (9)$$

where $A = \mathcal{P}_{SX}(0\,K)$ the extrapolated value of $\mathcal{P}_{SX}$ at 0 K and $B = d\mathcal{P}_{SX}(T)/dT$.

The uncertainty in $\mathcal{P}_{SX}(T)$ was determined from the propagated uncertainties of the different parameters derived from the experimental data.

The determination of polar free energy components of solvents adsorbed on solid surfaces was obtained using eqn (7) and the values of $\mathcal{P}_{SX}$ given in Table 3 and S4–S6. The representation of total free energy $\Delta G_a^0(T)$ (*n*-alkane) (Tables S4-S6) of n-alkanes adsorbed on solid materials as a function of parameter of $\mathcal{P}_{SX}$ *n*-alkanes denoted $\mathcal{P}_{S(n\text{-alkane})}$ give the *n*-alkanes-straight-line (Fig. 1) represented by the following equation:

$$(-\Delta G_a^0)(T)(n\text{-alkane}) = A\,\mathcal{P}_{S(n\text{-alkane})} + C \quad (10)$$

where A is a constant depending on the separation distance H and C a parameter function of temperature.

When a polar solvent (X) is adsorbed, it is then characterized by its representative geometric point with two coordinates $[\mathcal{P}_{SX};\ (-\Delta G_a^0)(T)(X)]$. The difference between the free energy $(-\Delta G_a^0)(T)(X)$ of the polar solvent and that of the fictive point located on the *n*-alkanes-straight-line having the same abscissa $\mathcal{P}_{SX}$ (Fig. 1), gives the corresponding polar free energy $(-\Delta G_a^p)(T)(X)$ of solvent X:

$$\left(-\Delta G_a^p\right)(X) = (-\Delta G_a^0)(X) - (A\,\mathcal{P}_{SX} + C) \quad (11)$$

Using the values of $\mathcal{P}_{SX}(T)$ given in Table 3 and those of free energy $(-\Delta G_a^0)$ of adsorption reported in Tables S4–S6, the polar free energy $\Delta G_a^p(T)$ of the adsorbed organic solvents on solid materials were then obtained. The new values of $\Delta G_a^p(T)$ of the various solvents adsorbed on alumina, titania, and MgO were given in Table 5 as a function of temperature.

Table 5 showed that the lowest values of free polar interaction $\Delta G_a^p(T)$ were obtained with the titanium dioxide, whereas MgO gave the highest $\Delta G_a^p(T)$. However, the values of $\Delta G_a^p(T)$ relative alumina are not so far from the those of magnesium oxide.

The determined free energy of adsorption of the polar solvents in Table 5 showed closest values for MgO and alumina very larger than those of titania then proving higher polar interaction for alumina and MgO.

The results showed in Table 5 were compared to those previously obtained without considering the thermal effect on the ionization energy and deformation polarizability.[1] It was observed in Table 6 an important deviation between the results of the two methods varying from 7% to 2665% (in the case of THF adsorbed on titania).

Serious consequences resulted from the above results leading to a higher disparity in the values of other surface thermodynamic parameters, particularly on the polar enthalpy and entropy of adsorption, and Lewis acid–base parameters of the solid substrates.

Table 4 Equations $\mathcal{P}_{SX}(T)$ of the different solvents adsorbed on solid materials with the extrapolated values of $\mathcal{P}_{SX}(0\ K)$ at 0 K and the corresponding slopes $d\mathcal{P}_{SX}(T)/dT$. Values of $\mathcal{P}_{SX}$ are expressed as ×J Å^6 K^{-1} mol^{-1} and T in K. The estimated standard deviations are bounded by: $\Delta\mathcal{P}_{SX}(0\ K) \leq 0.010$ (×10^{-54} J Å^6 mol^{-1}) and $\Delta(d\mathcal{P}_{SX}(T)/dT) \leq 0.1$ (×J Å^6 K^{-1} mol^{-1})

Alumina			
Solvents	Equation $\mathcal{P}_{SX}(T)$	$\frac{d\mathcal{P}_{SX}(T)}{dT}$ (×10^{-3})	$\mathcal{P}_{SX}(0\ K)$
n-Hexane	$\mathcal{P}_{SX}(T) = 0.0094T + 31.843$	9.4	31.843
n-Heptane	$\mathcal{P}_{SX}(T) = 0.0112T + 36.031$	11.2	36.031
n-Octane	$\mathcal{P}_{SX}(T) = 0.0135T + 41.711$	13.5	41.711
n-Nonane	$\mathcal{P}_{SX}(T) = 0.015T + 45.247$	15	45.247
CCl_4	$\mathcal{P}_{SX}(T) = 0.0077T + 30.696$	7.7	30.696
CH_2Cl_2	$\mathcal{P}_{SX}(T) = 0.0044T + 20.517$	4.4	20.517
Chloroform	$\mathcal{P}_{SX}(T) = 0.006T + 25.083$	6	25.083
Ether	$\mathcal{P}_{SX}(T) = 0.0068T + 24.866$	6.8	24.866
THF	$\mathcal{P}_{SX}(T) = 0.0058T + 21.491$	5.8	21.491
Ethyl acetate	$\mathcal{P}_{SX}(T) = 0.0079T + 24.196$	7.9	24.196
Toluene	$\mathcal{P}_{SX}(T) = 0.0077T + 30.27$	7.7	30.27
Titania			
Solvents	Equation $\mathcal{P}_{SX}(T)$	$d\mathcal{P}_{SX}(T)/dT$ (×10^{-3})	$\mathcal{P}_{SX}(0\ K)$
n-Hexane	$\mathcal{P}_{SX}(T) = 0.0191T + 54.481$	19.1	54.481
n-Heptane	$\mathcal{P}_{SX}(T) = 0.0225T + 61.502$	22.5	61.502
n-Octane	$\mathcal{P}_{SX}(T) = 0.027T + 71.085$	27	71.085
n-Nonane	$\mathcal{P}_{SX}(T) = 0.0298T + 77.028$	29.8	77.028
CH_2Cl_2	$\mathcal{P}_{SX}(T) = 0.0095T + 35.556$	9.5	35.556
Chloroform	$\mathcal{P}_{SX}(T) = 0.0128T + 43.483$	12.8	43.483
THF	$\mathcal{P}_{SX}(T) = 0.0118T + 36.454$	11.8	36.454
Ethyl acetate	$\mathcal{P}_{SX}(T) = 0.0158T + 41.333$	15.8	41.333
Acetone	$\mathcal{P}_{SX}(T) = 0.008T + 29.164$	8	29.164
Benzene	$\mathcal{P}_{SX}(T) = 0.014T + 45.856$	14	45.856
Nitromethane	$\mathcal{P}_{SX}(T) = 0.01T + 35.947$	10	35.947
Acetonitrile	$\mathcal{P}_{SX}(T) = 0.0058T + 22.658$	5.8	22.658
MgO			
Solvents	Equation $\mathcal{P}_{SX}(T)$	$d\mathcal{P}_{SX}(T)/dT$ (×10^{-3})	$\mathcal{P}_{SX}(0\ K)$
n-Hexane	$\mathcal{P}_{SX}(T) = 0.007T + 39.287$	7	39.287
n-Heptane	$\mathcal{P}_{SX}(T) = 0.0085T + 44.409$	8.5	44.409
n-Octane	$\mathcal{P}_{SX}(T) = 0.0106T + 51.378$	10.6	51.378
n-Nonane	$\mathcal{P}_{SX}(T) = 0.0118T + 55.708$	11.8	55.708
CH_2Cl_2	$\mathcal{P}_{SX}(T) = 0.0027T + 25.452$	2.7	25.452
Chloroform	$\mathcal{P}_{SX}(T) = 0.004T + 31.134$	4	31.134
Diethyl ether	$\mathcal{P}_{SX}(T) = 0.0048T + 30.556$	4.8	30.556
THF	$\mathcal{P}_{SX}(T) = 0.0041T + 26.386$	4.1	26.386
Ethyl acetate	$\mathcal{P}_{SX}(T) = 0.0062T + 29.842$	6.2	29.842
Acetone	$\mathcal{P}_{SX}(T) = 0.0023T + 21.053$	2.3	21.053
Acetonitrile	$\mathcal{P}_{SX}(T) = 0.0016T + 16.153$	1.6	16.153
Toluene	$\mathcal{P}_{SX}(T) = 0.0052T + 37.023$	5.2	37.023

The polar enthalpy ($-\Delta H_a^p$) and entropy ($-\Delta S_a^p$) of solvents adsorbed on solid surfaces were obtained from the variations of the free energy of adsorption against the temperature using the following relation:

Table 5 Variations of polar free energy $\Delta G_a^p(T)$ (kJ mol^{-1}) of adsorbed solvents on solid surfaces as a function of temperature. The relative error associated with $\Delta G_a^p(T)$ is less than 1%, as determined from chromatographic measurements

Alumina				
Temperature (K)	323.15	343.15	363.15	383.15
CCl_4	6.848	6.591	6.442	6.291
CH_2Cl_2	38.946	36.464	34.334	31.831
Chloroform	18.676	16.093	13.779	11.726
Ether	41.199	39.000	37.001	35.171
THF	40.653	38.187	36.030	34.111
Ethyl acetate	43.013	40.705	38.397	36.089
Toluene	18.913	17.415	16.269	15.598
Titania				
Temperature (K)	323.15	343.15	363.15	383.15
CH_2Cl_2	5.965	5.575	5.287	4.801
Chloroform	2.622	1.497	0.374	0.000
THF	4.122	2.800	1.480	0.167
Ethyl acetate	3.193	1.611	0.032	0.000
Acetone	4.943	3.228	1.515	0.000
Benzene	0.580	0.529	0.481	0.440
Nitromethane	9.723	8.353	6.985	5.619
Acetonitrile	3.610	1.506	0.000	0.000
MgO				
Temperature (K)	323.15	343.15	363.15	383.15
CH_2Cl_2	39.945	38.903	37.861	36.819
Chloroform	10.589	10.026	9.635	9.248
Diethyl ether	35.873	33.635	31.689	29.375
THF	21.071	18.283	15.806	13.596
Ethyl acetate	29.652	27.310	24.968	22.626
Acetone	46.707	44.062	41.716	39.541
Acetonitrile	46.573	43.625	41.094	38.803
Toluene	19.088	17.577	16.417	15.737

$$\Delta G_a^p(T) = \Delta H_a^p - T\Delta S_a^p \quad (12)$$

The values of the above thermodynamic variables were given in Table 7 compared to the previous results obtained without taking into account the thermal effect on the ionization energy and deformation polarizability of solvents.

The results in Table 7 led to the Lewis enthalpic acid–base constants K_A and K_D using the empirical relation (13):

$$-\Delta H^p = K_A \times DN + K_D \times AN \quad (13)$$

where AN and DN are, respectively, the electron donor and acceptor numbers of the polar molecule.[45,46]

The values of K_A and K_D of solids were deduced by drawing the variations of $\left(\frac{-\Delta S_a^p}{AN'}\right) = \omega_A\left(\frac{DN'}{AN'}\right) + \omega_D$ *versus* $\left(\frac{DN}{AN}\right)$ of polar solvents using eqn (14):

$$\left(-\frac{\Delta H^p}{AN}\right) = K_A\left(\frac{DN}{AN}\right) + K_D \quad (14)$$

The same procedure was used for the determination of the Lewis entropic acidic ω_A and basic ω_D constants of the various solid surfaces using eqn (15) or (16).

Table 6 Error percentage committed when the thermal effect of the chromatographic parameters is neglected in adsorbed solvents on alumina, titania and MgO

Alumina				
Temperature (K)	323.15	343.15	363.15	383.15
CCl_4	95.1	97.5	98.7	—
CH_2Cl_2	82.7	81.8	80.8	79.1
Chloroform	107.8	127.7	151.6	178.1
Ether	55.0	58.4	62.1	65.0
THF	1.1	2.5	3.4	4.9
Ethyl acetate	73.0	76.8	79.5	83.0
Toluene	114.3	120.4	123.6	123.6
Titania				
Temperature (K)	323.15	343.15	363.15	383.15
CH2Cl2	57.3	65.5	76.3	84.9
Chloroform	20.0	34.9	138.5	—
THF	84.9	136.5	279.7	2665.2
Ethyl acetate	24.6	50.0	2544.8	—
Acetone	16.9	26.0	55.9	—
Benzene	859.4	693.7	489.8	232.6
Nitromethane	6.9	8.0	9.6	11.8
Acetonitrile	27.8	67.6	—	—
MgO				
Temperature (K)	323.15	343.15	363.15	383.15
CH2Cl2	91.7	90.3	88.0	85.8
TCM	44.9	73.1	83.8	76.5
Diethyl ether	59.8	50.8	41.1	29.5
THF	9.4	36.8	70.4	111.8
Ethyl acetate	79.0	72.1	63.5	53.5
Acetone	66.3	53.4	39.2	23.5

$$\left(-\Delta S_a^p\right) = \omega_A DN' + \omega_D AN' \quad (15)$$

$$\left(\frac{-\Delta S_a^p}{AN'}\right) = \omega_A\left(\frac{DN'}{AN'}\right) + \omega_D \quad (16)$$

The Lewis enthalpic and entropic acid–base parameters were shown in Table 8 and compared to the previous results.

The results indicate that all three solid materials exhibit an amphoteric character with a predominance of basic behavior. Alumina shows the highest enthalpic and entropic Lewis acid and base constants, followed by MgO, whereas titania presents the lowest Lewis acid and base constants. The Lewis acid–base parameters of MgO and alumina are found to be very close, while titania displays K_A and K_D values approximately three times lower than those of alumina and MgO. Comparison with previous results[1] reveals comparable K_A and K_D values for alumina and titania, but significantly different values for MgO surfaces. Moreover, the discrepancy between the two methods becomes more pronounced for the entropic acid–base constants ω_A and ω_D. Overall, the present approach provides a more accurate quantification of the surface properties of solid materials.

Table 7 Comparison between the values of polar enthalpy ($-\Delta H_a^p$ in kJ mol^{-1}) and entropy ($-\Delta S_a^p$ in J K^{-1} mol^{-1}) of the various polar solvents adsorbed on the various solid obtained using the previous method[1] and the new method, with the error percentages of the previous method

Alumina						
	Previous results		New results		Error (%) on	Error (%) on
Solvents	$-\Delta S_a^p$(J K^{-1}mol^{-1})	$-\Delta H_a^p$(kJ mol^{-1})	$-\Delta S_a^p$(J K^{-1}mol^{-1})	$-\Delta H_a^p$(kJ mol^{-1})	$(-\Delta S_a^p)$	$(-\Delta H_a^p)$
CCl_4	6.2	2.314	9.1	9.7553	31.9	76.3
CH_2Cl_2	1.9	7.3421	117.4	76.843	98.4	90.4
$CHCl_3$	102.8	71.989	115.8	55.971	11.2	28.6
Diethyl ether	104.6	52.207	100.4	73.55	4.2	29.0
THF	88.8	69.683	108.9	75.711	18.5	8.0
Ethyl acetate	90.4	40.683	115.4	80.305	21.7	49.3
Toluene	94.9	71.036	55.4	36.628	71.3	93.9

Titanium dioxide						
	Previous results		New results		Error (%) on	Error (%) on
Solvents	$-\Delta S_a^p$(J K^{-1}mol^{-1})	$-\Delta H_a^p$(kJ mol^{-1})	$-\Delta S_a^p$(J K^{-1}mol^{-1})	$-\Delta H_a^p$(kJ mol^{-1})	$(-\Delta S_a^p)$	$(-\Delta H_a^p)$
CH_2Cl_2	30.7	12.146	18.9	12.084	62.4	0.5
$CHCl_3$	56.4	20.818	56.2	20.780	0.4	0.2
THF	10	23.277	65.9	25.423	84.8	8.4
Ethyl acetate	78.1	28.448	79	28.729	1.1	1.0
Acetone	85.4	32.518	85.7	32.635	0.4	0.4
Benzene	68.3	26.965	2.3	1.335	2869.6	1920.0
Nitromethane	68.5	31.846	68.4	31.829	0.1	0.1
Acetonitrile	104.6	37.37	105.1	37.586	0.5	0.6

MgO						
	Previous results		New results		Error (%) on	Error (%) on
Solvents	$-\Delta S_a^p$(J K^{-1}mol^{-1})	$-\Delta H_a^p$(kJ mol^{-1})	$-\Delta S_a^p$(J K^{-1}mol^{-1})	$-\Delta H_a^p$(kJ mol^{-1})	$(-\Delta S_a^p)$	$(-\Delta H_a^p)$
CH_2Cl_2	32.2	7.1665	52.100	56.781	38.2	87.4
$CHCl_3$	−60.5	−24.435	22.1	17.665	373.8	238.3
Diethyl ether	105.1	19.543	107.2	70.503	2.0	72.3
Ethyl acetate	71.9	17.038	124.5	61.159	42.2	72.1
THF	95.8	7.8791	117.100	67.493	18.2	88.3
Acetone	242	62.489	119.2	85.107	103.0	26.6
Acetonitrile	81.6	2.0138	129.2	88.148	36.8	97.7
Toluene	−13.8	15.211	56.1	37.003	124.6	58.9

4. Discussion

The temperature dependence of the ionization energy and deformation polarizability of solvents adsorbed on alumina, titania, and MgO induces significant variations in the surface thermodynamic properties, particularly in the polar component of the adsorption energy and the Lewis acid–base constants of the solid surfaces. Accordingly, a correction of the surface properties relative to the previous method was performed, clearly highlighting the strong influence of temperature on the thermodynamic parameters governing the Lewis acid–base behavior of these materials.

Table 8 Values of the enthalpic acid–base constants K_A and K_D and the entropic acid base constants ω_A and ω_D of the various solid surfaces with the corresponding acid–base ratios, using the new thermal method compared to the results of the previous method[1]

	Previous results			This work		
Lewis parameter	Alumina	Titania	MgO	Alumina	Titania	MgO
K_A	0.71	0.25	0.08	0.79	0.27	0.65
K_D	2.21	0.87	1.13	2.69	0.89	2.37
K_D/K_A	3.1	3.5	14	3.41	3.26	3.65
R^2	0.7301	0.9874	0.1722	0.9827	0.9895	0.9585
$10^3 \times \omega_A$	0.92	0.86	1.16	1.13	0.73	1.39
$10^3 \times \omega_D$	4.21	1.8	0.57	3.92	2.03	2.00
ω_D/ω_A	4.58	2.09	0.49	3.48	2.79	1.44
R^2	0.7739	0.9804	0.8126	0.973	0.9885	0.9754

The values of total free energy $-\Delta G_a^0(T)$ of different solvents adsorbed on solid surfaces given in Tables S4–S6 and those of the corresponding polar energy $-\Delta G_a^p(T)$ given in Table 5 led to determine the London dispersive energy of adsorbed solvents as a function of temperature using the following equation:

$$\Delta G_a^d(T) = \Delta G_a^0(T) - \Delta G_a^p(T) \quad (17)$$

The results are given in Table 9.

The original consequence of this new approach was the determination of the intermolecular distance $H(T)$ between the organic solvents and the solid materials as a function of temperature. Indeed, using eqn (4) and the values of London dispersive free energy $-\Delta G_a^d(T)$ of adsorption of solvents on the different solid surfaces given in Table 9 against the temperature, the values of the intermolecular distance $H(T)$ were obtained from the following Equations:

$$\left(-\Delta G_a^d(T)\right) = \frac{\mathcal{P}_{SX}(T)}{H(T)^6} \quad (18)$$

$$H(T) = \left[\frac{\mathcal{P}_{SX}(T)}{\left(-\Delta G_a^d(T)\right)}\right]^{1/6} \quad (19)$$

The values of $H(T)$ were given in Table 10.

The variations of $H(T)$ between the solvents and the solid substrates reported in Table 10 highlight a clear temperature effect on the intermolecular distance. A linear increase of $H(T)$ with increasing temperature is observed for *n*-alkanes, whereas a decrease of $H(T)$ is found for polar solvents. The results in Table 10 also reveal significant differences in intermolecular distances that strongly depend on the polarity and surface characteristics of the solid materials. In particular, the lowest $H(T)$ values are obtained for alumina, followed by MgO, while the highest values are observed for titania. This trend is consistent with the Lewis acid–base

Table 9 Variations of London dispersive energy $-\Delta G_a^d(T)$ (kJ mol^{-1}) of adsorbed solvents on solid surfaces as a function of temperature

Alumina				
Temperature (K)	323.15	343.15	363.15	383.15
n-Hexane	28.716	28.776	28.827	28.878
n-Heptane	31.857	31.774	31.692	31.609
n-Octane	35.117	34.813	34.510	34.207
n-Nonane	38.467	37.716	37.163	36.611
CCl_4	27.666	27.858	27.993	28.129
CH_2Cl_2	20.691	21.455	22.033	22.610
Chloroform	23.848	24.355	24.734	25.112
Ether	23.863	24.377	24.762	25.145
THF	21.575	22.277	22.808	23.338
Ethyl acetate	23.675	24.218	24.626	25.031
Toluene	47.776	47.508	46.754	45.523
Titania				
Temperature (K)	323.15	343.15	363.15	383.15
n-Hexane	12.233	11.145	10.061	8.981
n-Heptane	16.137	15.048	13.963	12.882
n-Octane	18.889	17.739	16.593	15.451
n-Nonane	21.792	20.513	19.239	17.968
CH_2Cl_2	4.902	3.994	3.089	2.186
Chloroform	8.045	7.073	6.102	5.134
THF	5.479	4.571	3.665	2.761
Ethyl acetate	7.640	6.700	5.760	4.821
Acetone	2.497	1.646	0.797	
Benzene	9.017	8.026	7.037	6.050
Nitromethane	5.093	4.183	3.276	2.370
MgO				
Temperature (K)	323.15	343.15	363.15	383.15
n-Hexane	28.716	28.776	28.827	28.878
n-Heptane	31.857	31.774	31.692	31.609
n-Octane	35.117	34.813	34.510	34.207
n-Nonane	38.467	37.716	37.163	36.611
CH_2Cl_2	20.718	21.478	22.056	22.631
Chloroform	23.925	24.424	24.800	25.172
Diethyl ether	23.764	24.284	24.678	25.066
THF	21.453	22.165	22.706	23.242
Ethyl acetate	23.625	24.171	24.585	24.992
Acetone	18.355	19.315	20.047	20.775
Acetonitrile	15.656	16.839	17.744	18.645
Toluene	27.215	27.443	27.611	27.774

Table 10 Variations of the intermolecular distance $H(T)$ (in Å) of the different solvents adsorbed on solid as a function of temperature

Alumina				
Temperature T (K)	323.15	343.15	363.15	383.15
n-Hexane	3.267	3.268	3.270	3.272
n-Heptane	3.280	3.284	3.289	3.293
n-Octane	3.309	3.317	3.325	3.333
n-Nonane	3.305	3.319	3.330	3.342
CCl_4	3.260	3.259	3.258	3.258
CH_2Cl_2	3.193	3.176	3.164	3.153
Chloroform	3.229	3.220	3.214	3.209
Ether	3.229	3.220	3.215	3.209
THF	3.205	3.190	3.180	3.171
Ethyl acetate	3.227	3.218	3.213	3.207
Toluene	2.871	2.877	2.887	2.903
Titania				
Temperature T (K)	323.15	343.15	363.15	383.15
n-Hexane	4.129	4.198	4.275	4.361
n-Heptane	4.026	4.078	4.134	4.194
n-Octane	4.021	4.068	4.118	4.172
n-Nonane	3.980	4.025	4.073	4.125
CH_2Cl_2	4.461	4.619	4.825	5.116
Chloroform	4.253	4.349	4.461	4.596
THF	4.409	4.549	4.724	4.957
Ethyl acetate	4.272	4.372	4.488	4.629
Acetone	4.831	5.183	5.853	—
Benzene	4.213	4.299	4.398	4.515
Nitromethane	4.443	4.595	4.790	5.060
MgO				
Temperature T (K)	323.15	343.15	363.15	383.15
n-Hexane	3.363	3.364	3.365	3.366
n-Heptane	3.376	3.380	3.383	3.387
n-Octane	3.406	3.413	3.420	3.427
n-Nonane	3.401	3.414	3.425	3.436
CH_2Cl_2	3.291	3.246	3.068	3.066
Chloroform	3.327	3.308	3.133	3.135
Diethyl ether	3.325	3.272	2.882	2.900
THF	3.300	3.226	2.996	3.020
Ethyl acetate	3.324	3.263	2.802	2.817
Acetone	3.254	3.167	2.660	2.672
Acetonitrile	3.195	3.085	2.564	2.575
Toluene	3.353	3.327	3.098	3.105

properties of the solid surfaces, as alumina exhibits the highest acid–base constants, leading to shorter intermolecular distances due to stronger van der Waals and specific interactions.

The temperature dependence of deformation polarizability reflects the progressive softening of the electronic cloud under thermal excitation, leading to enhanced electronic deformation at the solid–molecule interface. Simultaneously, the decrease in ionization energy with temperature indicates a reduction of the electronic potential barrier, facilitating charge displacement and polarization. Together, these effects amplify dispersive and polarization-induced interactions, thereby modifying surface energy, adsorption strength, and Lewis acid–base characteristics of oxide materials.

5. Conclusions

The surface properties of oxide materials such as alumina, titania, and magnesium oxide were determined using a refined approach that explicitly accounts for the temperature dependence of the ionization energy and deformation polarizability of probe molecules, and consequently of the surface thermodynamic parameters of solid materials. Although only slight variations in ionization energy and deformation polarizability of organic solvents were observed with temperature, these changes resulted in significant differences in the calculated surface properties of the oxides. In particular, marked discrepancies were found in the Lewis acid–base constants obtained using the present thermal method compared with those derived from the previous

approach, which neglected temperature effects on the dispersive and polar components of the adsorption energy.

The substantial differences observed in the intermolecular distances between solvents and the various solid substrates further confirm the superiority of the proposed method, as they reflect a more physically consistent description of solid–molecule interactions.

Overall, these findings highlight the critical importance of incorporating temperature-dependent electronic and polarizability effects when evaluating surface reactivity, adhesion, and interfacial interactions. From a broader materials science perspective, this work establishes a fundamental link between molecular-scale properties of probe molecules and macroscopic surface behavior, providing new insights for the rational design of functional materials, surface coatings, and nanostructured interfaces with tailored thermodynamic and interfacial properties.

Conflicts of interest

The author declares no conflicts of interest.

Data availability

The data presented in this study are available in the article.

Supplementary information (SI): the data supporting the findings of this study are provided within the article and its SI. The SI contains detailed physicochemical datasets and parameters used throughout the analysis. Specifically, Table S1 reports the corrected donor (DN′) and acceptor (AN′) numbers, along with dipole moments (μ), of the investigated organic solvents, characterizing their Lewis acid–base properties. Table S2 presents the temperature-dependent deformation polarizability of both solvents and solid materials, while Table S3 provides the corresponding temperature-dependent ionization energies. Tables S4–S6 compile the temperature-dependent standard Gibbs free energies of adsorption for solvents on alumina, titania, and MgO surfaces, respectively, as determined by inverse gas chromatography. These datasets form the basis for the thermodynamic and molecular interaction analyses presented in the manuscript. In addition, a comprehensive list of abbreviations and symbols is provided to ensure clarity and reproducibility of the methodology, including definitions of all thermodynamic, molecular, and surface parameters employed in the study. See DOI: https://doi.org/10.1039/d6lf00006a.

References

1 T. Hamieh, New Progress on London Dispersive Energy, Polar Surface Interactions, and Lewis's Acid–Base Properties of Solid Surfaces, *Molecules*, 2024, **29**, 949, DOI: 10.3390/molecules29050949.
2 D. T. Sawyer and D. J. Brookman, Thermodynamically based gas chromatographic retention index for organic molecules using salt-modified aluminas and porous silica beads, *Anal. Chem.*, 1968, **40**, 1847–1850, DOI: 10.1021/ac60268a015.
3 C. Saint-Flour and E. Papirer, Gas-solid chromatography. A method of measuring surface free energy characteristics of short carbon fibers. 1. Through adsorption isotherms, *Ind. Eng. Chem. Prod. Res. Dev.*, 1982, **21**, 337–341, DOI: 10.1021/i300006a029.
4 C. Saint-Flour and E. Papirer, Gas-solid chromatography: Method of measuring surface free energy characteristics of short fibers. 2. Through retention volumes measured near zero surface coverage, *Ind. Eng. Chem. Prod. Res. Dev.*, 1982, **21**, 666–669, DOI: 10.1021/i300008a031.
5 J. B. Donnet, S. J. Park and H. Balard, Evaluation of specific interactions of solid surfaces by inverse gas chromatography, *Chromatographia*, 1991, **31**, 434–440.
6 E. Brendlé and E. Papirer, A new topological index for molecular probes used in inverse gas chromatography for the surface nanorugosity evaluation, 2. Application for the Evaluation of the Solid Surface Specific Interaction Potential, *J. Colloid Interface Sci.*, 1997, **194**, 217–224.
7 E. Brendlé and E. Papirer, A new topological index for molecular probes used in inverse gas chromatography for the surface nanorugosity evaluation, 1. Method of Evaluation, *J. Colloid Interface Sci.*, 1997, **194**, 207–216.
8 T. Hamieh and J. Schultz, New approach to characterise physicochemical properties of solid substrates by inverse gas chromatography at infinite dilution. I. II. And III, *J. Chromatogr. A*, 2002, **969**, 17–47, DOI: 10.1016/S0021-9673(02)00368-0.
9 J. B. Donnet, E. Custodéro, T. K. Wang and G. Hennebert, Energy site distribution of carbon black surfaces by inverse gas chromatography at finite concentration conditions, *Carbon*, 2002, **40**, 163–167, DOI: 10.1016/S0008-6223(01)00168-3.
10 E. Papirer, E. Brendlé, F. Ozil and H. Balard, Comparison of the surface properties of graphite, carbon black and fullerene samples, measured by inverse gas chromatography, *Carbon*, 1999, **37**, 1265–1274, DOI: 10.1016/S0008-6223(98)00323-6.
11 J. F. Gamble, R. N. Davé, S. Kiang, M. M. Leane, M. Tobyn and S. S. Y. Wang, Investigating the applicability of inverse gas chromatography to binary powdered systems: An application of surface heterogeneity profiles to understanding preferential probe-surface interactions, *Int. J. Pharm.*, 2013, **445**, 39–46.
12 H. Balard, D. Maafa, A. Santini and J. B. Donnet, Study by inverse gas chromatography of the surface properties of milled graphites, *J. Chromatogr. A*, 2008, **1198–1199**, 173–180.
13 T. Hamieh, Study of the temperature effect on the surface area of model organic molecules, the dispersive surface energy and the surface properties of solids by inverse gas chromatography, *J. Chromatogr. A*, 2020, **1627**, 461372.
14 T. Hamieh, A. A. Ahmad, T. Roques-Carmes and J. Toufaily, New approach to determine the surface and interface thermodynamic properties of H-β-zeolite/rhodium catalysts by inverse gas chromatography at infinite dilution, *Sci. Rep.*, 2020, **10**, 20894.

15 T. Hamieh, New methodology to study the dispersive component of the surface energy and acid–base properties of silica particles by inverse gas chromatography at infinite dilution, *J. Chromatogr. Sci.*, 2022, **60**, 126–142, DOI: 10.1093/chromsci/bmab066.
16 T. Hamieh, Some Irregularities in the Evaluation of Surface Parameters of Solid Materials by Inverse Gas Chromatography, *Langmuir*, 2023, **39**, 17059–17070, DOI: 10.1021/acs.langmuir.3c01649.
17 T. Hamieh, Inverse Gas Chromatography to Characterize the Surface Properties of Solid Materials, *Chem. Mater.*, 2024, **36**(5), 2231–2244, DOI: 10.1021/acs.chemmater.3c03091.
18 A. Voelkel, B. Strzemiecka, K. Adamska and K. Milczewska, Inverse gas chromatography as a source of physiochemical data, *J. Chromatogr. A*, 2009, **1216**, 1551.
19 Z. Y. Al-Saigh and P. Munk, Study of polymer-polymer interaction coefficients in polymer blends using inverse gas chromatography, *Macromolecules*, 1984, **17**, 803.
20 S. K. Papadopoulou and C. Panayiotou, Thermodynamic characterization of poly(1,1,1,3,3,3-hexafluoroisopropyl methacrylate) by inverse gas chromatography, *J. Chromatogr. A*, 2012, **1229**, 230.
21 P. Coimbra, M. S. N. Coelho and J. A. F. Gamelas, Surface characterization of polysaccharide scaffolds by inverse gas chromatography regarding application in tissue engineering, *Surf. Interface Anal.*, 2019, **51**(11), 1070–1077.
22 J. Kołodziejek, A. Voelkel and K. Heberger, Characterization of hybrid materials by means of inverse gas chromatography and chemometrics, *J. Pharm. Sci.*, 2013, **102**, 1524.
23 H. M. Ryan, J. G. Douglas and W. Rupert, Inverse Gas Chromatography for Determining the Dispersive Surface Free Energy and Acid–Base Interactions of Sheet Molding Compound-Part II 14 Ligno-Cellulosic Fiber Types for Possible Composite Reinforcement, *J. Appl. Polym. Sci.*, 2008, **110**, 3880–3888.
24 P. N. Jacob and J. C. Berg, Acid-base surface energy characterization of microcrystalline cellulose and two wood pulp fiber types using inverse gas chromatography, *Langmuir*, 1994, **10**, 3086–3093.
25 M. G. Carvalho, J. M. R. C. A. Santos, A. A. Martins and M. M. Figueiredo, The Effects of Beating, Web Forming and Sizing on the Surface Energy of *Eucalyptus globulus* Kraft Fibres Evaluated by Inverse Gas Chromatography, *Cellulose*, 2005, **12**, 371–383.
26 T. Hamieh, The Effect of Temperature on the Surface Energetic Properties of Carbon Fibers Using Inverse Gas Chromatography, *Crystals*, 2024, **14**, 28, DOI: 10.3390/cryst14010028.
27 T. Hamieh, London Dispersive and Lewis Acid-Base Surface Energy of 2D Single-Crystalline and Polycrystalline Covalent Organic Frameworks, *Crystals*, 2024, **14**, 148, DOI: 10.3390/cryst14020148.
28 H. Chtourou, B. Riedl and B. V. Kokta, Surface characterizations of modified polyethylene pulp and wood pulps fibers using XPS and inverse gas chromatography, *J. Adhes. Sci. Technol.*, 1995, **9**, 551–574.
29 V. I. Bogillo, V. P. Shkilev and A. Voelkel, Determination of surface free energy components for heterogeneous solids by means of inverse gas chromatography at finite concentrations, *J. Mater. Chem.*, 1998, **8**, 1953–1961.
30 S. C. Das, Q. Zhou, D. A. V. Morton, I. Larson and P. J. Stewart, Use of surface energy distributions by inverse gas chromatography to understand mechanofusion processing and functionality of lactose coated with magnesium stearate, *Eur. J. Pharm. Sci.*, 2011, **43**, 325–333.
31 S. C. Das and P. J. Stewart, Characterising surface energy of pharmaceutical powders by inverse gas chromatography at finite dilution, *J. Pharm. Pharmacol.*, 2012, **64**, 1337–1348.
32 W. Bai, E. Pakdel, Q. Li, J. Wang, W. Tang, B. Tang and X. Wang, Inverse gas chromatography (IGC) for studying the cellulosic materials surface characteristics: A mini review, *Cellulose*, 2023, **30**, 3379–3396, DOI: 10.1007/s10570-023-05116-9.
33 S. Dong, M. Brendlé and J. B. Donnet, Study of solid surface polarity by inverse gas chromatography at infinite dilution, *Chromatographia*, 1989, **28**, 469–472.
34 T. Hamieh, Temperature Dependence of the Polar and Lewis Acid–Base Properties of Poly Methyl Methacrylate Adsorbed on Silica via Inverse Gas Chromatography, *Molecules*, 2024, **29**, 1688, DOI: 10.3390/molecules29081688.
35 J. F. Gamble, M. Leane, D. Olusanmi, M. Tobyn, E. Supuk, J. Khoo and M. Naderi, Surface energy analysis as a tool to probe the surface energy characteristics of micronized materials—A comparison with inverse gas chromatography, *Int. J. Pharm.*, 2012, **422**, 238–244.
36 H. E. Newell, G. Buckton, D. A. Butler, F. Thielmann and D. R. Williams, The use of inverse gas chromatography to measure the surface energy of crystalline, amorphous, and recently milled lactose, *Pharm. Res.*, 2001, **18**, 662–666.
37 H. E. Newell and G. Buckton, Inverse gas chromatography: Investigating whether the technique preferentially probes high energy sites for mixtures of crystalline and amorphous lactose, *Pharm. Res.*, 2004, **21**, 1440–1444.
38 R. Ho, S. J. Hinder, J. F. Watts, S. E. Dilworth, D. R. Williams and J. Y. Y. Heng, Determination of surface heterogeneity of D-mannitol by sessile drop contact angle and finite concentration inverse gas chromatography, *Int. J. Pharm.*, 2010, **387**, 79–86.
39 R. Calvet, S. Del Confetto, H. Balard, E. Brendlé and J. B. Donnet, Study of the interaction polybutadiene/fillers using inverse gas chromatography, *J. Chromatogr. A*, 2012, **1253**, 164–170.
40 S. K. Papadopoulou, G. Dritsas, I. Karapanagiotis, I. Zuburtikudis and C. Panayiotou, Surface characterization of poly(2,2,3,3,3-pentafluoropropyl methacrylate) by inverse gas chromatography and contact angle measurements Eur, *Polym. J.*, 2010, **46**, 202–208.
41 G. S. Dritsas, K. Karatasos and C. Panayiotou, Investigation of thermodynamic properties of hyperbranched poly(ester amide) by inverse gas chromatography, *J. Polym. Sci. Polym. Phys.*, 2008, **46**, 2166–2172.

42 D. L. Chung, *Carbon Fiber Composites*, Butterworth-Heinemann, Boston, MA, USA, 1994, pp. 3–65, ISBN: 978-0-08-050073-7, DOI: 10.1016/C2009-0-26078-8.
43 J. B. Donnet and R. C. Bansal, *Carbon Fibers*, Marcel Dekker, New York, NY, USA, 2nd edn, 1990, p. 584, DOI: 10.1201/9781482285390.
44 Y. Liu, Y. Gu, S. Wang and M. Li, Optimization for testing conditions of inverse gas chromatography and surface energies of various carbon fiber bundles, *Carbon Lett.*, 2023, **33**, 909–920, DOI: 10.1007/s42823-023-00472-9.
45 A. Pal, A. Kondor, S. Mitra, K. Thua, S. Harish and B. B. Saha, On surface energy and acid–base properties of highly porous parent and surface treated activated carbons using inverse gas chromatography, *J. Ind. Eng. Chem.*, 2019, **69**, 432–443, DOI: 10.1016/j.jiec.2018.09.046.
46 P. K. Basivi, T. Hamieh, V. Kakani, V. R. Pasupuleti, G. Sasikala, S. M. Heo, K. S. Pasupuleti, M.-D. Kim, V. S. Munagapati, N. S. Kumar, J.-H. Wen and C. W. Kim, Exploring advanced materials: Harnessing the synergy of inverse gas chromatography and artificial vision intelligence, *TrAC, Trends Anal. Chem.*, 2024, **173**, 117655, DOI: 10.1016/j.trac.2024.117655.
47 C. Kemball and E. K. Rideal, The adsorption of vapours on mercury I) Non –polar substances, *Proc. R. Soc. London, Ser. A*, 1946, **187**, 53–73.
48 J. H. De Boer and S. Kruyer, Entropy and mobility of adsorbed molecules I) Procedure; atomic gases on charcoal, *Proc. K. Ned. Akad. Wet., Ser. B*, 1952, **55**, 451–463.
49 M. Laib and D. M. Mittleman, Terahertz spectroscopy of liquid n-alkanes: Temperature dependence, *J. Infrared, Millimeter, Terahertz Waves*, 2010, **31**(9), 1015–1024.
50 *Semiconductors: Data Handbook*, ed. O. Madelung, Springer, 3rd edn, 2004.
51 J. Barthel and R. Buchner, Dielectric spectroscopy of ethers over temperature, *J. Solution Chem.*, 1995, **24**(12), 1311–1327.
52 R. Buchner, G. Hefter and J. Barthel, Dielectric relaxation of polar aprotic solvents: Temperature and frequency dependence, *J. Phys. Chem. A*, 1999, **103**(1), 1–9.
53 J. Barthel, R. Buchner and M. Münsterer, Static and dynamic dielectric permittivity of acetonitrile, *Chem. Phys. Lett.*, 1995, **240**(1–3), 193–200.
54 J. Barthel and R. Buchner, Dielectric properties of aromatic hydrocarbons versus temperature, *J. Mol. Liq.*, 1995, **67**(1), 1–12.
55 A. S. Barker and A. J. Sievers, Optical studies of Al_2O_3 dielectric properties vs temperature, *Rev. Mod. Phys.*, 1975, **47**(2), S1–S179.
56 J. H. Parker, Dielectric response of TiO_2 as a function of temperature, *Phys. Rev.*, 1967, **155**(3), 712–714.
57 R. A. Marcus, Electrostatic free energy and other properties of states having nonequilibrium polarization, *J. Chem. Phys.*, 1956, **24**(5), 979–989, DOI: 10.1063/1.1742723.
58 J. K. Parker and C. E. Brion, Absolute photoabsorption cross-sections and oscillator strengths for valence-shell transitions in acetone and ethanol, *Chem. Phys.*, 1978, **31**(2), 317–333, DOI: 10.1016/0301-0104(78)85118-1.
59 T. W. Bentley and P. v. R. Schleyer, The Grunwald–Winstein equation, *Adv. Phys. Org. Chem.*, 1977, **14**, 1–67, DOI: 10.1016/S0065-3160(08)60294-2.
60 B. K. P. Scaife and A. W. Lyons, Dielectric permittivity and pVT data of some n-alkanes, *Proc. R. Soc. London, Ser. A*, 1980, **370**, 193–212.
61 B. K. P. Scaife and A. W. Lyons, Density and dielectric polarizability of n-alkane liquids, *Ber. Bunsenges. Phys. Chem.*, 1990, **94**, 758–765.
62 U. Kaatze, Complex permittivity of nitromethane as function of temperature and frequency, *J. Chem. Phys.*, 1989, **90**, 3071–3077.
63 R. Buchner and J. Barthel, Dielectric relaxation of halogenated methanes as function of temperature, *J. Mol. Liq.*, 1995, **63**, 21–39.
64 J. Barthel and R. Buchner, Dielectric spectroscopy of ethers over temperature, *J. Solution Chem.*, 1995, **24**, 1311–1327.
65 P. Issofa, E. Njabon, S. Njankwa, T. Tchamba and A. Emadak, Kinetic and mechanistic insights into the atmospheric hydrogen abstraction of 3-Hydroxybutanal by chlorine, *Chem. Rev. Lett.*, 2026, 11–16, DOI: 10.22034/crl.2025.532470.1648.
66 R. Behjatmanesh-Ardakani and H. Imanov, DFT study on the mechanism of benzimidazole synthesis from phenylenediamine and formic acid: Activation energies and transition states' locations, *Chem. Rev. Lett.*, 2025, **8**(6), 1188–1199, DOI: 10.22034/crl.2025.537649.1665.
67 M. Haqgu, Z. Rostami and A. Mengboev, DFT investigation of aflatoxin B1 adsorption on vacancy-defective graphene: electronic properties and sensing potential, *Chem. Rev. Lett.*, 2025, **8**(6), 1258–1268, DOI: 10.22034/crl.2025.544347.1683.
68 R. Omer, A. Anwar, Y. Hussein, H. K. I. Sultan, H. K. Ismail, A. F. Hamasdiq and R. Kareem, Obaid Synthesis and DFT-guided evaluation of PPy-$ZnFe_2O_4$@Fe_3O_4 nanocomposite for pharmaceutical adsorption, *J. Chem. Lett.*, 2026, 240–255, DOI: 10.22034/jchemlett.2025.554966.1361.
69 M. A. Rafiee and M. Javaheri, Theoretical Study of Benzoquinone Derivatives as Organic Cathode Materials in Lithium-Ion Batteries, *J. Chem. Lett.*, 2025, **6**(3), 166–174, DOI: 10.22034/jchemlett.2025.516569.1295.
70 A.-K. Kabi, DFT-Based Insights into Carboxylic Acid Acidity: Correlating pKa with Free Energy and Vibrational Signatures, *J. Chem. Lett.*, 2025, **6**(3), 212–222, DOI: 10.22034/jchemlett.2025.543299.1340.